Hierarchical porous Polybenzimidazole microsieves: An efficient architecture for anhydrous proton transport via Poly-ionic Liquids

Parashuram Kallem[†§¥], Martin Drobek[§], Anne Julbe[§], Erik J. Vriezekolk[¥], Reyes Mallada[†‡] and Maria Pilar Pina[†‡],*

† Institute of Nanoscience of Aragon. Department of Chemical & Environmental Engineering, University of Zaragoza. Edif. I+D+i, Campus Rio Ebro. C/Mariano Esquillor, 50018. Zaragoza, Spain.

§ IEM (Institut Européen des Membranes), UMR 5635 (CNRS-ENSCM-UM), Université de Montpellier, CC047, Place Eugène Bataillon, 34095 Montpellier, France

¥ Membrane Science & Technology, Mesa+ Institute for Nanotechnology, University of Twente, P.O. Box 217, 7500 AE Enschede, The Netherlands

‡ Networking Research Center on Bioengineering, Biomaterials and Nanomedicine, CIBER-BBN, 50018 Zaragoza, Spain

KEYWORDS:, Liquid induced phase separation micromolding, hierarchical porous polybenzimidazole microsieves, Poly imidazolium ionic liquids, Cross linking, , Anhydrous proton transport, The influence of the porous support architecture.

ABSTRACT: Liquid induced phase separation micromolding (LIPSμM) has been successfully used for manufacturing hierarchical porous polybenzimidazole (HPBI) microsieves (42-46% porosity, 30-40 μm thick) with specific pore architecture (pattern of macropores ~ 9 μm in size perforated dispersed in a porous matrix with 50-100 nm pore size). Using these microsieves, proton exchange membranes were fabricated by infiltration of 1-H-3-vinyl imidazolium bis(trifluoromethanesulfonyl)imide liquid and divinylbenzene (as cross-linker) followed by *in-situ* UV polymerization. Our approach relies on the separation of the ion conducting function from the structural support function. Thus, the polymeric ionic liquid (PIL) moiety plays the role as proton conductor, while the HPBI microsieve ensures the mechanical resistance of the system. The influence of the porous support architecture on both proton transport performance and mechanical strength has been specifically investigated by means of comparison with straight macro-porous (36% porosity) and randomly nano-porous (68% porosity) PBI counterparts. The most attractive results were obtained with poly[1-(3H-imidazolium)ethylene]bis(trifluoromethanesulfonyl)imide polymeric ionic liquid (PIL) cross-linked with 1 % divinylbenzene supported on HPBI membranes with 21 μm thick skin layer, achieving conductivity values up to 85 $mS \cdot cm^{-1}$ at 200 °C under anhydrous conditions and in the absence of mineral acids.

1. INTRODUCTION

High temperature proton exchange membranes (HTPEM) are receiving increasing attention in PEM fuel cells (PEMFC) field because of higher reaction kinetics, enhanced CO-tolerance and generally improved overall performance[1-3]. Since the first successful application of polybenzimidazole (PBI) membranes as electrolytes[4], PBIs have been often reported as promising materials for PEMs due to their excellent thermal stability and outstanding mechanical properties[5-11]. In parallel, ionic liquids (ILs) are non-volatile, non-flammable, and exhibit good chemical and thermal stability, as well as high ionic conductivity. All these properties are clearly beneficial for HTPEM applications. Hence, ILs based PEMs have recently led to promising results in emerging research studies[2, 12,9-10, 13-18].

In this work, a novel asymmetric PBI matrix has been designed and used as a skeleton for the IL- based electrolyte membrane. The use of highly porous PBI membranes has been already described for PEMFC applications[7-8, 10]. Owing to their high specific surface area for either acid doping or conducting phase embedding, the overall electrolyte performance was notably increased. Jheng et al[8]. proposed highly porous (83.1 vol.%) asymmetric PBI supports through a soft-templating method using 1-ethyl-3-methylimidazolium bis(trifluoromethanesulfonyl)imide, [EMIm][TFSI], as porogen agent. Proton conductivity values above 60 $mS \cdot cm^{-1}$ at 160 °C were reported upon phosphoric acid doping (23.6 as doping level). Van de Ven et al[10]. described the fabrication of macrovoid-free randomly porous PBI membranes (65.6 vol.%) impregnated with H-3-methylimidazolium bis(trifluoromethanesulfonyl) imide, [HMIm][TFSI], ionic liquid. The proton conductivity and power density of such PBI/IL membranes were 1.86 $mS \cdot cm^{-1}$ at 190 °C and 0.039 $W \cdot cm^{-2}$ at 150 °C, respectively. However, ILs tend to drain out from the membranes after long-time operation[19]. In this respect, polymerization of ILs emerges as an attractive option for ILs based PEMs in terms of safety, stability and mechanical properties. Polymeric ionic liquids

(PILs)[17, 20-24] are likely to provide a continuous route with ionic character, and at the same time retain some of the unique properties of ILs.

Very recently, our group[7] has investigated the *in-situ* UV polymerization of 1-H-3-vinylimidazolium bis(trifluoromethanesulfonyl)imide [HVIm][TFSI] onto a highly random porous PBI sponge-like support (above 75 vol%) achieving conductivity values above 300 mS cm^{-1} at 200 °C under anhydrous conditions. Unfortunately, the excellent conduction performance was hampered by the brittleness of the membranes. This finding was in line with previously reported studies confirming that high porosity leads to a decrease of both storage modulus and tensile strength[8, 25-26]. Similar drawbacks are commonly alleviated by using of supports with optimized pore architecture. In particular, better PIL filling and enhanced conduction would be expected with a pattern of perforated macropores having straight well defined geometries, as the effective pathways become shorter compared to porous supports with random pores shapes, sizes and locations. An attractive option relies on the application of microsieves. These porous materials were introduced over a decade ago[27], and since then, the span of their applications has been growing steadily[28-30]. The main features of microsieves rely on the presence of straight-through, high density, uniform and well-ordered pores between 0.5 and 10 μm in diameter[31-32].

Over the last decade Wessling group[33-35] has extensively developed phase separation micromolding (PSμM) techniques. In PSμM, the phase separation of a polymer solution is combined with replication of structures on a micro-to submicrometer scale. Compared to the thermally induced PSμM process progressed by Vogelaar et al[36], in liquid induced phase separation micromolding (LIPSμM), the phase separation proceeds mainly through an exchange of solvent and non-solvent taking place between the polymer solution and coagulation bath[31, 36]. In a step further, the manufacturing of membranes with a variety of

pore sizes (down to 0.2 μm) from single mold has been fully investigated by using a solvent-shrinkage approach[37].

Herein, we propose an innovative HTPEM concept consisting of hierarchically structured PIL channels embedded in a HPBI microsieve. Although at first sight, the intrinsic porosity of the HPBI support may seem useless or even unwanted, the inner surface created by the intrinsic porosity enable for ionic liquid confinement and offers additional pathways for proton transport through the PIL network. Furthermore, such intrinsic porosity might offer a solution for problems derived from both the fluidity and poor mechanical strength of PILs. To the best of our knowledge, the combination of HPBI microsieves, prepared by LIPSμM, and in-situ polymerization of ionic liquid moieties for HTPEM applications is attempted for the first time in this work. Such PIL-HPBI electrolyte membranes are expected to retain the advantageous features (fast infiltration process and high network connectivity) of both perforated straight pores and intrinsic random pores of the HPBI microsieves. Compared to sponge-like supports or dense PBI microsieves, an outperforming performance is expected for such PIL-HPBI systems as higher and well-connected PIL loadings are achievable without sacrificing the mechanical resistance. Thus, a comprehensive physicochemical and electrochemical characterization of these proton conducting membranes before and after cross-linking has been accomplished up to 200 °C under anhydrous conditions. Particular emphasis is devoted to the analysis of the skin layer effect and to the influence of PBI pore architecture on the exhibited conduction performance.

2. EXPERIMENTAL SECTION

2.1 Materials

All chemical reagents and solvents listed hereafter were used as received: poly[2,2-(m-phenylene)-5,5-bibenzimidazole] (PBI Fumion APH Ionomer, Mw 59,000-62,000,

Fumatech), LiCl (99 wt%, Sigma-Aldrich), poly(vinylpyrrolidone) (PVP) K30 (M_w = 40000, Fluka), PVP K90 (M_w = 360000, Fluka), 1-H-3-vinylimidazoliumbis(trifluoromethane sulfonyl)imide (98 wt%, SOLVIONIC), divinylbenzene (80 wt%, Sigma-Aldrich), 2-hydroxy-2-methylpropiophenone (97 wt%, Sigma-Aldrich), N-methyl-2-pyrrolidone (NMP anhydrous, 99.5 wt%, Sigma-Aldrich).

2.2 Structured mold

The structured Si mold was prepared by photolithographic techniques and cryogenic deep reactive ion etching (DRIE) on the Si wafer according to method published elsewhere[37]. It comprised uniform pyramid shaped pillars (mold named as "type P") with base diameter ~ 8 µm, height ~ 20 µm, located every 15 µm with center to center periodicity.

2.3 PBI solution preparation

PBI was used as a polymer for membrane fabrication. Polymer solutions were prepared according to a protocol published in the literature[7], by mixing 4.5 g of PBI powder, 1 g of LiCl, 1 g of PVP K30, 1 g of PVP K90 and 42.5 g of NMP at 175 °C for 24 h to obtain polymer solutions 15% wt. of solids . Polymer solutions were then outgassed for 2 h in order to remove all air bubbles. Addition of PVP controls macrovoid formation upon phase separation process while LiCl stabilizes the PBI solution.

2.4 PBI microsieves preparation

PBI microsieves were prepared by liquid induced phase separation micromolding (LIPSµM) method, as schematically shown in Figure 1. Polymer solution composed of PBI, PVP, LiCl and NMP was poured onto the structured silicon mold (Figure.1A) and cast with a custom-made casting device.

The casting device with an adjustable casting knife is shown in supporting information (Figure S1). Distances between the casting knife and the mold were adjusted within 1 µm accuracy with micrometric screws. Casting distances (*cd*) were altered between 3 and 25 µm above pillar level. After casting, the mold with polymer solution was immersed for 30 min at room temperature (RT) into the coagulation bath (Fig. 1B) containing a NMP/water solution (50/50 wt%). Then, it was transferred into a non-solvent bath (pure water) at RT for 30 minutes in order to wash out NMP traces (Fig. 1C).

The solidified PBI membrane, peeled off from the mold, was first immersed in ethanol for 30 min (Fig. 1D)., and then in hexane for another 30 min in order to ensure complete water removal. Finally, in order to remove all volatile compounds, the as-formed membranes were sandwiched between two glass plates and placed in an oven at 150 °C. After the casting procedure, molds were cleaned by NMP and rinsed with acetone.

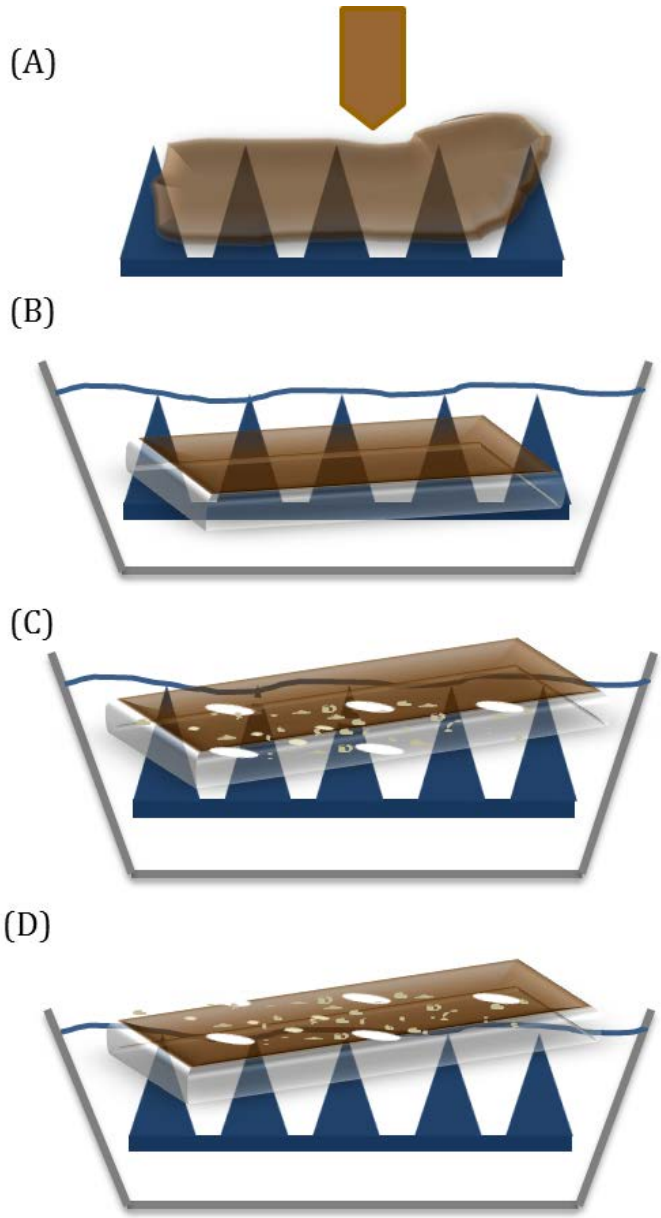

Figure 1. Schematic representation of liquid induced phase separation micromolding (LIPµM): (A) solution casting on structured mold, (B) system immersion in a NMP/H_2O solution (50/50 wt.%), (C)&(D) system immersion in pure water and ethanol, respectively.

Different types of hierarchically structured PBI (HPBI) microsieve supports were fabricated by adjusting the casting distance (see Table 1). In fact, the nomenclature adopted for microsieves description includes the casting distance value.

Table 1. Casting parameters used for the fabrication of HPBI microsieve supports with a P-type mold.

HPBI microsieve code	Casting distance cd (µm)
P-3µm	3± 1
P-5µm	5± 1
P-15µm	15±1
P-25µm	25±1

2.5 Polymer electrolyte membranes preparation

Polymer electrolyte membranes (PEMs) were prepared by infiltration of PBI with monomeric ionic liquid (MIL) 1-H-3-vinylimidazolium bis(trifluoromethane sulfonyl)imide (H-VIM TFSI) as previously published by our research group[7] (see Supporting information for the procedure, Figure S2). Monomeric ionic liquid (MIL) was first melted at 50 °C and then placed in contact with HPBI microsieve support previously dried under vacuum at 120 °C and 100 mbar. Subsequently, the system was placed under vacuum for 1 h to remove any air bubbles and thus ensure complete infiltration of the MIL into the HPBI microsieve support. This process was conducted by pouring the MIL on the HPBI surface at 100 °C under vacuum (160 mbar). The membrane was then removed out from the filter holder and the excess of ionic liquid on the membrane surface was wiped off with a tissue. Finally, 2-hydroxy-2-methylpropiophenone was added on the membrane top surface to initiate the photopolymerization process. For the polymerization, the composite membrane surface was exposed to UV lamp irradiation (Vilber Lourmat, with an intensity of 2.4 mW cm^{-2} and wavelength ~365 nm) for 2 hours on each side. Three types of cross-linked PIL-HPBI

membranes were prepared by varying the amount of cross-linking agent divinylbenzene: from 0.2 to 1.0 mol % (referred to the MIL). After polymerization, the composite membranes were gently wiped from any residuals with lab paper and acetone. The amount of PIL in the membranes was determined by weight measurements.

2.6 Characterization methods

2.6.1 Porosity

The porosity of the as-prepared HPBI microsieve supports was evaluated by immersion in n-butanol for 2h according to the protocol published elsewhere[38]. The porosity (ε) was calculated using following equation:

$$\varepsilon\,(\%) = \frac{\boldsymbol{w_B/\rho_B}}{\boldsymbol{w_M/\rho_M} + \boldsymbol{w_B/\rho_B}} \times \mathbf{100}$$

where w_B is the amount of absorbed n-butanol, $\boldsymbol{\rho}_B$ the density of n-butanol, w_M the weight of HPBI microsieve support and $\boldsymbol{\rho}_M$ its density.

2.6.2 Scanning Electron Microscopy (SEM)

The morphology and thickness of as-prepared HPBI microsieves and derived PIL-HPBI membranes were investigated by Scanning Electron Microscopy (SEM, JSM 6010LA operating at 5kV). The reported thickness values correspond to average values measured on 3 different samples at least. SEM samples were dried under vacuum at 60 °C for 15 h and coated with a thin gold layer (Balzer Union SCD 040 sputtering at 210 V and 13 mA, during 180 s in 10 mbar Ar atmosphere). Both pore diameters and their periodicity were measured by using SemAfore software.

2.6.3 Atomic Force Microscopy (AFM)

AFM measurements have been carried out in tapping mode using a NSG30 ND-MDT tip (Multimode 8 system, Veeco/Bruker) with force constant around 22-100 N/m.

2.6.4 Transmission Electron Microscopy (TEM)

Membranes were embedded in epoxy resin, and ultrathin slices (~ 50 nm thick) were cut with an ultramicrotome (Leica EM UC7) at room temperature. The as-prepared slices were placed on TEM copper grids with carbon film, and analysed by Transmission Electron Microscopy (Tecnai T20 - FEI Company) at a working voltage of 200kV. TEM Bright Field Images were acquired with a side-mounted Veleta CCD Camera.

2.6.5 Infrared Spectroscopy (FTIR)

ATR-FTIR analyses (Bruker VERTEX 70 with Golden Gate ATR from 4000 to 600 cm^{-1}, 256 scans, and resolution of 4 cm^{-1}) were performed at room temperature to monitor the photo-polymerization reaction and to investigate any possible changes on: *i)* protonation site of the poly-cationic backbone, i.e. poly[1-(3H-imidazolium)ethylene]; *ii)* vibrational spectrum of trifluoromethane sulfonyl)imide anion originating from ionic interactions, and *iii)* hydrogen bonding interactions between the benzimidazole groups in PBI and the poly[1-(3H-imidazolium)ethylene]bis(trifluoromethanesulfonyl)imide.

2.6.6 Thermogravimetric analyses (TGA)

Thermogravimetric analyses (Q500 IR TA instrument) were used to evaluate the composition and thermal behaviour of PIL-HPBI membranes with or without any cross-linker. Studies were conducted with 4-5 mg samples, in the temperature range from 25 °C to 900 °C with a heating rate of 2°C/min under N_2 atmosphere.

2.6.7 Mechanical properties

The Young's modulus and tensile strength of the PIL-HPBI (P1-9-25µm) membranes were analyzed by extensional rheology (Anton Paar rheometer MCR 301 equipped with Universal Extensional Fixture UXF12). The temperature was controlled at 25 ^{o}C (CTD180 Peltier system). The tested samples (4x1 cm^2) were cut in different areas of the membranes. For a given membrane composition (cross–linker amount), the reported values of mechanical parameters correspond to average values 3 different samples at least.

2.6.8 Impedance spectroscopy

Proton conductivity of membranes prepared with and without any cross-linker was measured by electrochemical impedance spectroscopy (ESI- Agilent 4294A precision impedance analyzer in the range 40 Hz- 110 MHz). Membranes were sandwiched between two gold electrodes and resistance through the plane was measured in anhydrous conditions, using high purity N_2 (> 99.998%) as a sweep gas (100 cm^3 STP/min). Measurements were performed every 10°C from 70 °C to 200 °C in a closed home-made stainless-steel conductivity cell PTFE lined inside provided with annular gold electrodes (11 mm outlet and 6.5 mm inlet diameter), as described in our previous works[18, 39]. Proton conductivity *(*σ in $mS{\cdot}cm^{-1}$) was calculated from measured resistance values (R in Ohms) using the equation $\sigma = z/RA$ where *z* is the membrane thickness in cm, and A is the electrodes surface area in cm^2. Electrolyte resistance was derived from the real impedance-axis intercept of the Nyquist plot (see Figure S3 of the supporting information). The activation energy for ionic conduction was calculated assuming Arrhenius-type dependence.

3. RESULTS AND DISCUSSION

3.1 Fabrication of Hierarchical PBI microsieves (HPBI) by LIPSµM

The main characteristics of the prepared microsieves are presented in Table 2. Both macropores height and total thickness of the asymmetric HPBI microsieve mainly depend on the casting distance (cd). Accordingly, the cd was altered between 3 and 25 µm above pillar level. The skin layer thickness increases with increasing cd and the nominal macropore height (~19.5 µm) could be obtained when cd exceeds 15 µm.

Table 2. Main characteristics of the HPBI microsieves fabricated by LIPSµM for this work

Microsieve code	Macropore dimensions (µm)		Periodicity (µm)	Thickness z (µm)		Porosity ε (%)		
	Diameter*	Height		Total	Skin layer	Total	Intrinsic[#]	Intrinsic/Macro
P-3µm	9.1±0.1	12.1±0.1	14.9±0.1	12.4±1	-	61.2	53.8	7.2
P-5µm	8.7±0.1	15.5±0.1	15.4±0.1	15.8±1	0.3±0.2	57.1	49.7	6.7
P-15µm	8.9±0.1	19.5±0.1	15.5±0.1	30.6±1	11.1±02	46.1	38.7	5.2
P-25µm	8.9±0.1	19.5±0.1	15.5±0.1	40.2±1	21.1±02	42.5	35.1	4.7

*mold side; [#]evaluated by subtracting the nominal macro porosity, i.e.7.4%, from total ε.

Moreover it has been found out that the obtained porosity depends on the skin layer thickness (Table 2) and it decreases for thicker skin layers. The highest porosity (~ 60%) was obtained for membranes with almost no skin layer (P-3µm and P-5µm). However, these membranes

have not been used further due to handling constraints. In comparison, mechanically more stable membranes, i.e. P-15µm and P-25 µm, exhibit the porosity of 46.1%, 42.5 %, respectively.

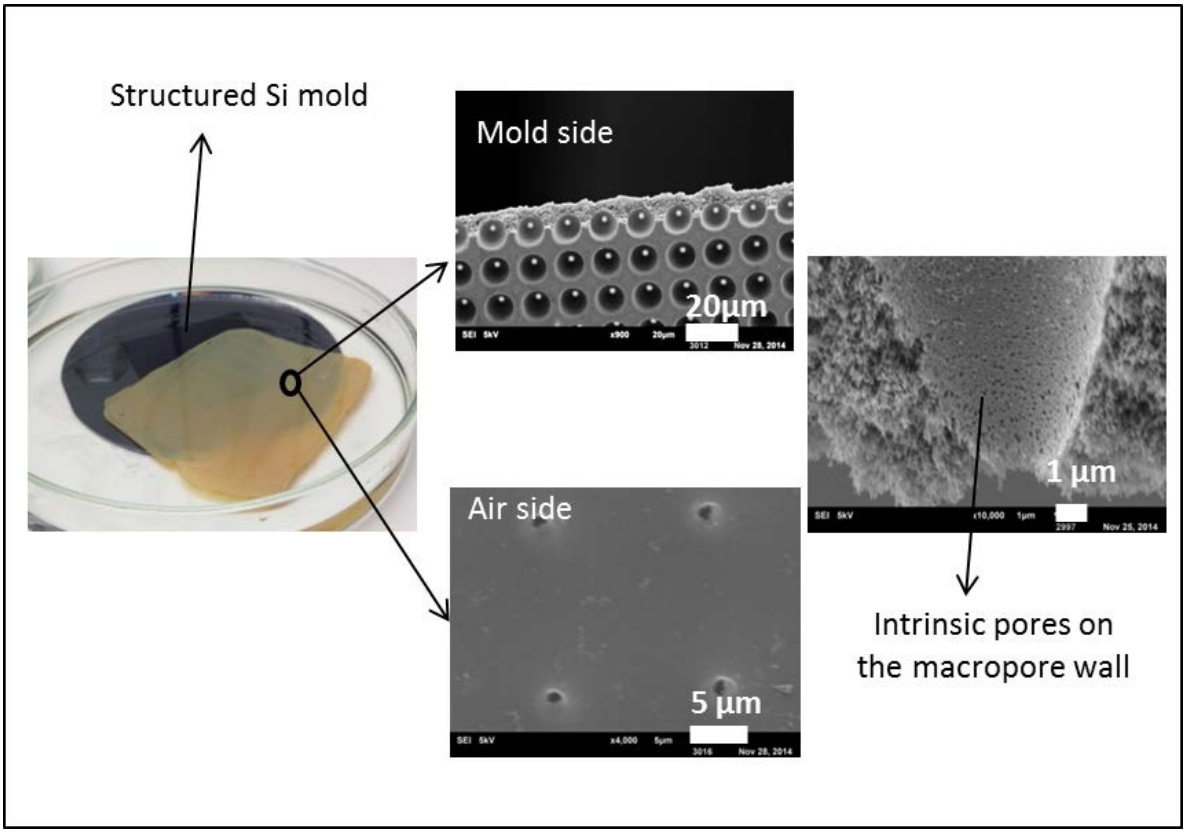

Figure 2. Pyramidal type pillar structured Si-mold used for the fabrication of HPBI. SEM images of P-5µm type microsieves: mold side, air side and cross-section.

Pyramidal type pillar structured Si-mold and SEM images of the as-prepared HPBI microsieves (air side, mold side and cross-section with intrinsic pores of 50-100 nm) are displayed in Figure 2. It must be noted that the straight-through macropores are generated by pillar perforation of the Si-mold, while the small (intrinsic) pores result from phase inversion process[35, 37]. SEM observations (see Figure 3) clearly confirm that the cast polymer adapts the structure of the structured mold. as published in the literature in LIPSµM [31, 33, 37], two types of shrinkages have to be considered for the polymer film on the mold: in-plane/lateral and thickness/perpendicular shrinkage. Thickness shrinkage occurs at a greater level than lateral

shrinkage. It permits film perforation and results in completely open microstructure. On the other hand, lateral shrinkage is responsible for film loosening from the mold, thus facilitating its release.

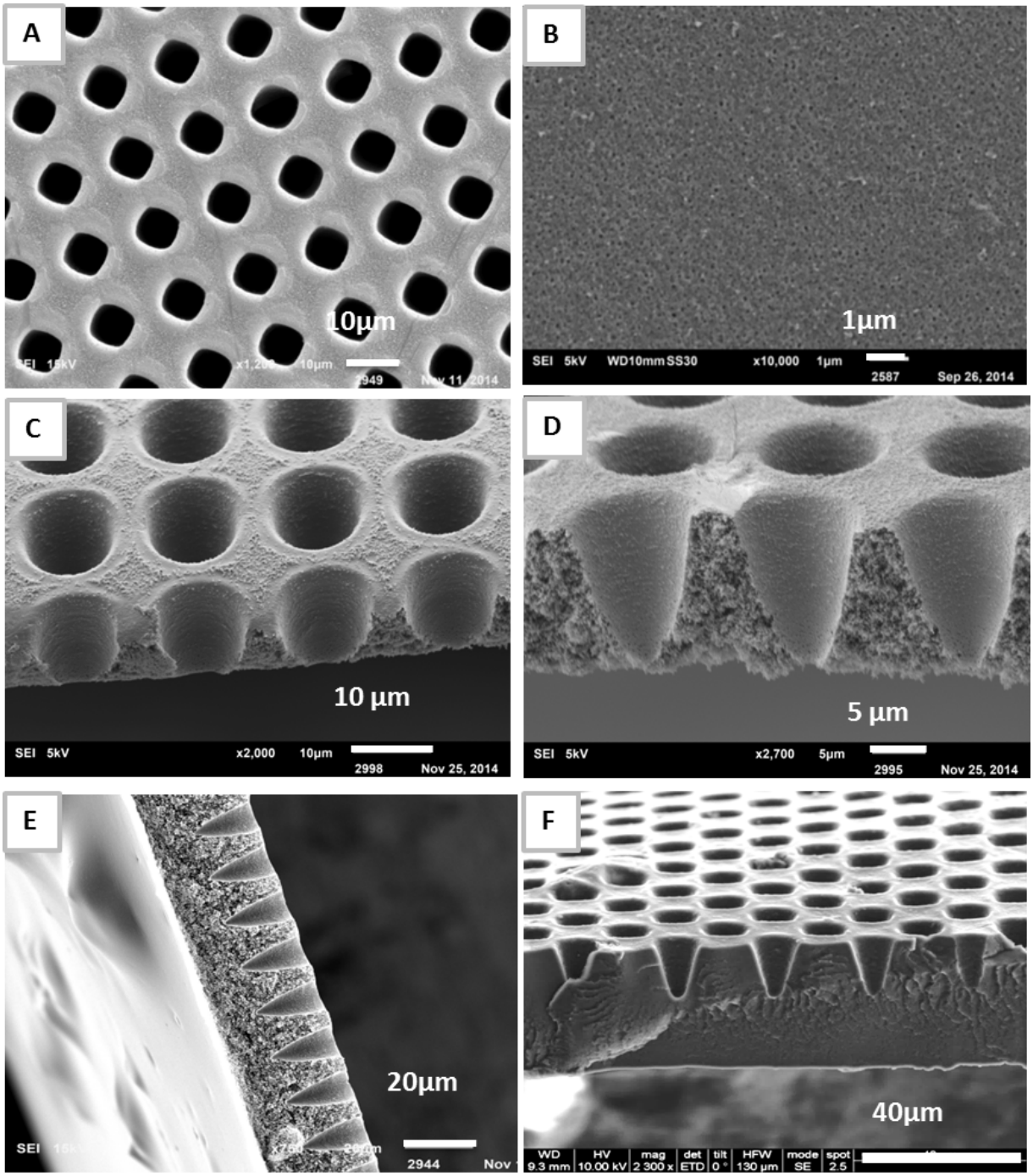

Figure 3. SEM images of HPBI microsieve with different skin layer thicknesses: A) P-25µm surface mold side; B) P-25µm surface air side; C) P-3µm cross-section; D) P-5µm cross-section; E) P-15µm cross-section; F) P-25µm cross-section.

These shrinkages yielded microsieves with perforated macropores of slightly different size compared to the pillars diameters of the mold[34]. Figure 3C-F reveal that skin layer thickness decreased with decreasing cd and the pillars did perforate through the whole film thickness (Figure 3C and 3D) at the minimum applied cd, i.e. 3 and 5 µm, respectively. SEM observations of both P-15µm and P-25µm microsieves (Figure 3E and F) evidenced perforated macropores with similar dimensions (height ~19 µm and periodicity ~15 µm) for both samples with a skin layer thickness of ~11 and ~21 µm, respectively.

3.2 Pore filling –PIL uptake

Due to its high proton conductivity, low water uptake values and high thermal stability[7], the monomeric ionic liquid (MIL) 1-H-3-vinylimidazolium bis(trifluoromethanesulfonyl)imide has been selected as a precursor for the preparation of PIL-HPBI composite membranes. Reported contact angle value for PBI films[40] (26° ± 0.13) makes the MIL an appropriate wetting liquid for efficient pore filling. The MIL viscosity was 14.3 mPa at 50 °C and 8.6 mPa at 100 °C[40]. Therefore, the infiltration process was conducted at 100 °C for ensuring complete pore filling.

Table 3 summarizes the list of prepared PIL-HPBI polymer electrolyte membranes (PEMs) with and without any cross-linker (CL). The nomenclature adopted for the electrolyte membrane description includes both the HPBI microsieve code and the CL percentage in the MIL solution. Thus, P-25µm-0%CL and P-15µm-0%CL membranes were prepared by introduction of MIL into P-25µm and P-15µm microsieves respectively without any cross-linker. On the other hand, P-25µm-0.2%CL, P-15µm-0.2%CL and P-25µm-0.5%CL, P-15µm-0.5%CL and P-25µm-1%CL, P-15µm-1%CL membranes were based on MIL with 0.2, 0.5 and 1.0 mol % CL respectively. In order to evaluate the influence PBI pore architecture on PIL uptake and conduction properties, PIL samples supported on randomly porous PBI

(PIL/RPBI-1%CL) membranes and on dense PBI microsieve (PIL/SPBI-1%CL) were separately prepared according to our previous works[7, 40].

Table 3. Main characteristics of the PEMS prepared for this work

PEM code	Thickness z (µm)	CL content (mol %)	PIL content (wt %)		
			Theoretical[1]	Exp[2]	TGA
P-25µm-PA	45.1±1	-	-	310[3]	
P-25µm-0%CL	45.6±1	0	42.7	63.3	65
P-25µm-0.2%CL	43.5±1	0.2	45.0	59.4	65
P-25µm-0.5%CL	44.1± 1	0.5	45.2	54.6	46
P-25µm-1%CL	45.1±1	1.0	47.5	49.5	43
P-15µm-0%CL	32.5±1	0	43.8	67.4	-
P-15µm-0.2%CL	33.1±1	0.2	43.4	59.6	-
P-15µm-0.5%CL	34.2±1	0.5	47.5	49.7	-
P-15µm-1%CL	34.0±1	1.0	47.2	46.2	-
PIL/SPBI-1%CL[4]	24.0±1	1.0	55.4	58.5	59.3
PIL/RPBI-1%CL[5]	120.0±3	1.0	82.5	86.5	78.6

[1]theoretical value based on PIL density and membrane porosity; [2]experimental value based on gravimetry measurements; [3]PA content in wt.% of PA, equivalent to a 9.5 doping level; [4]Data from [40]; [5]Data from [7].

Finally, in order to assess the electrochemical performance of PIL-PBI PEMs, a phosphoric acid (PA) doped P-25µm membrane (denoted as P-25µm-PA) was prepared by HPBI immersion in 11 M phosphoric acid solution for 24h at 80 °C, and was also studied. Table 3 shows that the PIL uptake of PEMs seems to depend on the PBI support architecture for values in the range 46 - 87 %. When considering P-15µm and P-25µm microsieves, the experimental PIL content values (based on gravimetry and TGA measurements-if applicable) were always higher than theoretical values with the exception of 1%CL samples.

This phenomenon was probably caused by difficulty in wiping the excess PIL from the membrane surface. It has been confirmed that the amount of PIL uptake into the HPBI microsieves after the crosslinking procedure is lower than in the absence of any CL. This effect is mainly attributed to the restriction of relatively high viscous MIL+CL mixture during its infiltration into the intrinsic porosity of the HPBI supports. In fact, this intrinsic porosity of the support is 4.7-5.2 folds higher than its nominal macroporosity, i.e. 7.4 vol% (see Table 2).

SEM analysis of PIL-HPBI PEMs is displayed in Figure 4. The key factor for PEMs performance relies on both uniform and complete filling of HPBI pores with PIL. The SEM images of PIL-HPBI PEMs prepared with and without any CL are shown in Figures 4A and 4B, respectively. In particular, the indistinguishable boundary layer between the PIL and the walls of the perforated porous HPBI microsieve has been observed. Although an excess of the PIL is noticed on the surface (P-25µm-0%CL, Figure 4A), it correlates well with the PIL loadings listed in Table 3. The entire and uniform filling of HPBI pores with PIL without any detactable cracks or defects is clearly evidenced in Figure 4C.

ATR-FTIR spectra have been used to corroborate the successful polymerization of MIL into the support and to explore any possible interaction between the PIL and the PBI microsieves.

Accordingly, the spectra of pure MIL, PIL, HPBI, and PIL-HPBI have been recorded (Figure 5). The presence of vinyl group in the MIL was observed in the region 1665-1630 cm^{-1} assigned to the stretching vibration of in-plane $CH=CH_2$ bending (Figure 5A). The absence of the characteristic peaks these vinyl monomers in PIL and PIL-HPBI confirms successful polymerization. The degree of MIL conversion to PIL was above 97% after 2 h of UV light exposure in good agreement with our previous studies[40].

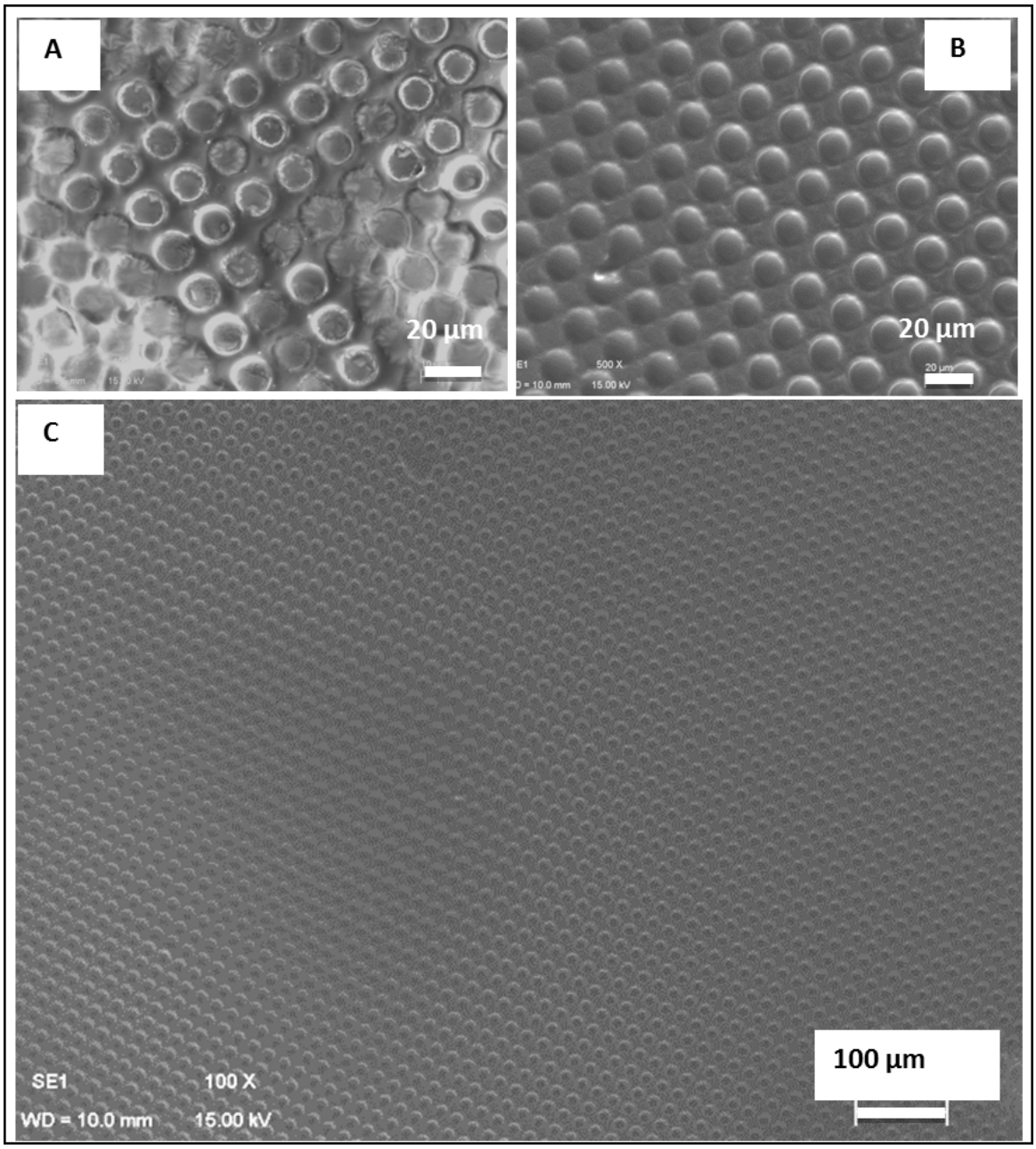

Figure 4. SEM images of HPBI microsieves after pore filling: A) P-25µm-0%CL; B) P-25µm-1%CL at high magnification (500x); and C) P-25µm-0%CL at low magnification (100x).

The intense peaks between 1400 and 1000 cm^{-1} (Figure 5A), characteristics for O=S=O and S-N-S vibration modes in bis(trifluoromethanesulfonyl)imide [TFSI] anion[40-41], remain unaltered for both PIL and PIL-HPBI samples. On the contrary, the broad band centred at 1608 cm^{-1} corresponding to aromatic C=C and C=N stretching modes, and the peak at 1539 cm^{-1}, resulting from in-plane ring vibrations of substituted benzimidazole (Figure 5A), are clearly diminished for the PIL-HPBI composite. The very broad band in the region 3700-2400 cm^{-1} is attributed to the free N-H stretching and to N-H···H, and H_2O···H hydrogen bonds interactions (see Figure 5B). These distinctive features, although notably less intense due to the hydrophobic nature of the PIL, are also depicted on the PIL-HPBI spectrum. The peak centered at 3059 cm^{-1}, assigned to the stretching modes of aromatics CH groups and clearly observed for HPBI sample, is notably suppressed for PIL-HPBI. These observations provide evidence on the interactions between the benzimidazole rings of PBI and the poly-cationic chains.

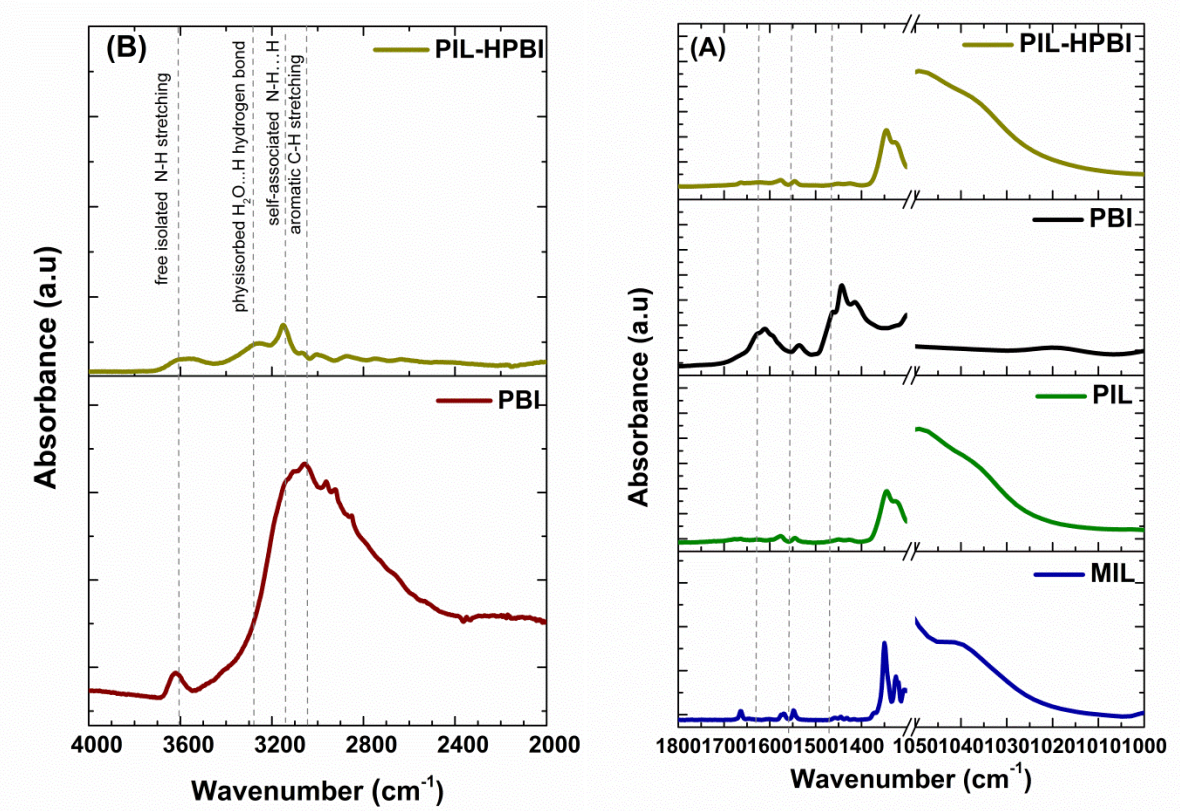

Figure 5. ATR-FTIR of PIL-HPBI composite membranes versus MIL, PIL and PBI counterparts: (A) 1800 - 1000 cm^{-1} region; (B) 4000 - 2000 cm^{-1} region.

3.3 Thermal and mechanical stability of PIL-HPBI membranes

An important design criterion for HT- PEMs is their thermal stability. Figure 6 shows the TGA and DTG thermograms of both pure PIL and composite PIL-HPBI membranes. The first weight loss, registered at temperatures below 200 °C corresponds to both residual water and traces of the photoinitiator[7] (4.5 to 8.9 wt %). The pure PIL decomposition is centred at around 405 °C (weight loss between 315 to 450 °C). On the other hand, the decomposition of PIL inside the porous HPBI matrix takes place within a wider temperature range, i.e. 320 - 540 °C. It can be observed that the onset temperature for decomposition is also shifted to higher values for cross-linked membranes (particularly with 0.5 and 1%CL). In addition, a distinctive shoulder at temperatures above 440 °C, and up to 510 °C is observed for all

composite samples, whatever the CL content. This behaviour is attributed to hydrogen bonding interactions between PIL and the confining PBI matrix, already evidenced by FTIR (Figure 5). In general, the obtained thermograms are in good agreement with those described in the literature for PEMs containing PBI and IL/PIL[7, 9-10, 42]. All the composite PIL-HPBI membranes are stable up to 300 °C, which is far above the operating temperature for HT PEMFCs.

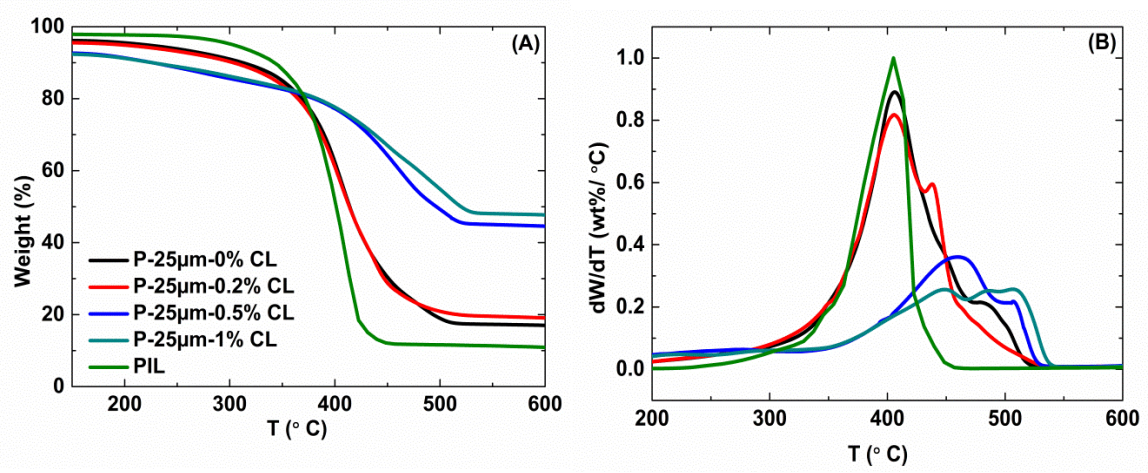

Figure 6. A) TGA and B) DTG thermograms of PIL based membranes (pure PIL behaviour also represented for comparison purposes).

The mechanical properties of the composite PIL-HPBI membranes were measured at room conditions, i.e. ambient RH and 25 °C (see Table 4). As essential requirements for practical operation of PEM rely on their mechanical stability, both high storage modulus and low swelling values are pursued[43]. Thus, the present work aims to improve the dimensional stability issues related to PIL-based membranes by using HPBI microsieves as structural supports. The pristine HPBI microsieve, i.e P-25µm sample, appears quite rigid with Young's modulus and tensile stress about 0.2 ±0.021 GPa and 0.9±0.7 MPa, respectively. However, both parameters are notably improved upon in situ polymerization of ionic liquid moieties. Thus, the evaluated Young's modulus of P-25µm-0%CL was 0.9 ± 0.04 GPa, which is about

more than 4 folds higher than the reported values for pure PIL[7, 17]. Furthermore, the mechanical strength of composite PIL-HPBI membranes increased moderately (77% in Young modulus and 112% in tensile stress) when cross-linking the polycationic network. The strain-stress curves, see Figure S4 of the supporting information, show that all the PIL−SPBI membranes exhibited a glassy nature.

Among the tested samples, P-25μm-1%CL membrane presented the maximum Young modulus and tensile stress values (1.6 ± 0.02 GPa and 5.3 ± 0.5 MPa, respectively). These values are 8 times higher in Young modulus and more than 4 times higher in tensile stress than those for PIL supported on randomly porous PBI (85% in porosity) [7], denoted as PIL/RPBI-1%CL. These values are also clearly superior to the characteristic values for acid-doped PBI[42] and Nafion115[44] membranes. Above all, the mechanical behaviour of P-25μm-1%CL sample was clearly outstanding during handling and assembly of the electrochemical cell.

Table 4. Mechanical properties of the PEMs prepared for this work

PEM code	Young Modulus (GPa)	Tensile Stress (MPa)
P-25µm-0%CL	0.9 ± 0.04	2.5 ± 0.5
P-25µm-0.2%CL	1.2 ±0.01	3.4 ± 0.3
P-25µm-0.5%CL	1.4 ± 0.07	4.1 ± 0.8
P-25µm-1%CL	1.6 ± 0.02	5.3 ± 0.5
PIL/RPBI-1%CL	0.19±0.09	1.21±0.03
PIL[*]	0.21±0.03	-
Dense PBI[**]	0.081	9.4
P-25µm[***]	0.2 ±0.02	0.9±0.7

[*]Data from[7]; [**]Data from dense PBI membrane after H_3PO_4 doping[42];
[***] Pristine HPBI microsieve as reference.

3.4 Electrochemical performance of PIL-HPBI electrolytes

3.4.1 Crosslinking effect

The proton conductivity measured for all the composite PIL-HPBI membranes as a function of temperature is presented in Figure 7A. Measurements performed for the pristine HPBI microsieve under anhydrous conditions confirmed its negligible conductivity, i.e. 0.73 $mS \cdot cm^{-1}$ at 150 °C. As can be seen, the proton conductivity increases with temperature. This phenomenon is associated with the viscosity reduction of the poly cation (poly[1-(3H-imidazolium)ethylene)[9, 45]. The proton conductivity of P-25µm-0%CL membranes increases from 22.2 $mS \cdot cm^{-1}$ to 69.6 $mS \cdot cm^{-1}$ when temperature increases from of 70 °C to 150 °C, respectively. These values are 5-6 times higher than those registered for phosphoric acid doped HPBI membrane (σ = 4.3 $mS \cdot cm^{-1}$ to 13.2 $mS \cdot cm^{-1}$ in the same temperature range). In addition, it has been reported that phosphoric acid-doping diminishes the mechanical strength of PBI[46-49]. Hence, prefilling HPBI supports with MIL followed by its in-situ polymerization enables the synthesis of proton conducting phosphoric acid-free electrolyte membrane operating at 150 °C under anhydrous conditions.

An increased amount of CL initiates a significant decrease in the proton conductivity. For the P-25µm-0.2%CL membrane, the maximum proton conductivity at 150 °C was 61.9 $mS \cdot cm^{-1}$; whereas at the same temperature, P-25µm-0.5%CL and P-25µm-1%CL membranes exhibited proton conductivities values limited at 54.7 $mS \cdot cm^{-1}$ and 47.3 $mS \cdot cm^{-1}$, respectively. These results could be explained by the effect of more a pronounced cross-linking which results in restrict chain mobility and thus lower PEM proton-conduction performance[7, 50-51]. Moreover, the cross-linker applied, i.e. divinylbenzene, is weak electrochemical in nature.

For the sake of further investigation of the proton conduction properties, activation energy (Ea) for proton transport was evaluated by using Arrhenius type dependence (see Figure 7.B

and Table S1 of the supporting information). As expected, due to the loss in long-range segmental motion, Ea slightly increases with the % of cross-linker ranging the values from 17.1 kJ·mol^{-1} for P-25μm-0%CL up to 21.8 kJ·mol^{-1} for P-25μm-1%CL. These values are also comparable with those values reported for ionic liquid and PBI blends[9, 42, 52].

Some replica conductivity measurements were also performed for both heating (from 70 to 150 °C) and cooling (from 150 to 70 °C) cycles in order to clarify whether any water adsorption influenced the conductivity of the PEMs[53]. It has been confirmed (see Figure S5 of the supporting information) that conduction performance shows a thermal reversibility.

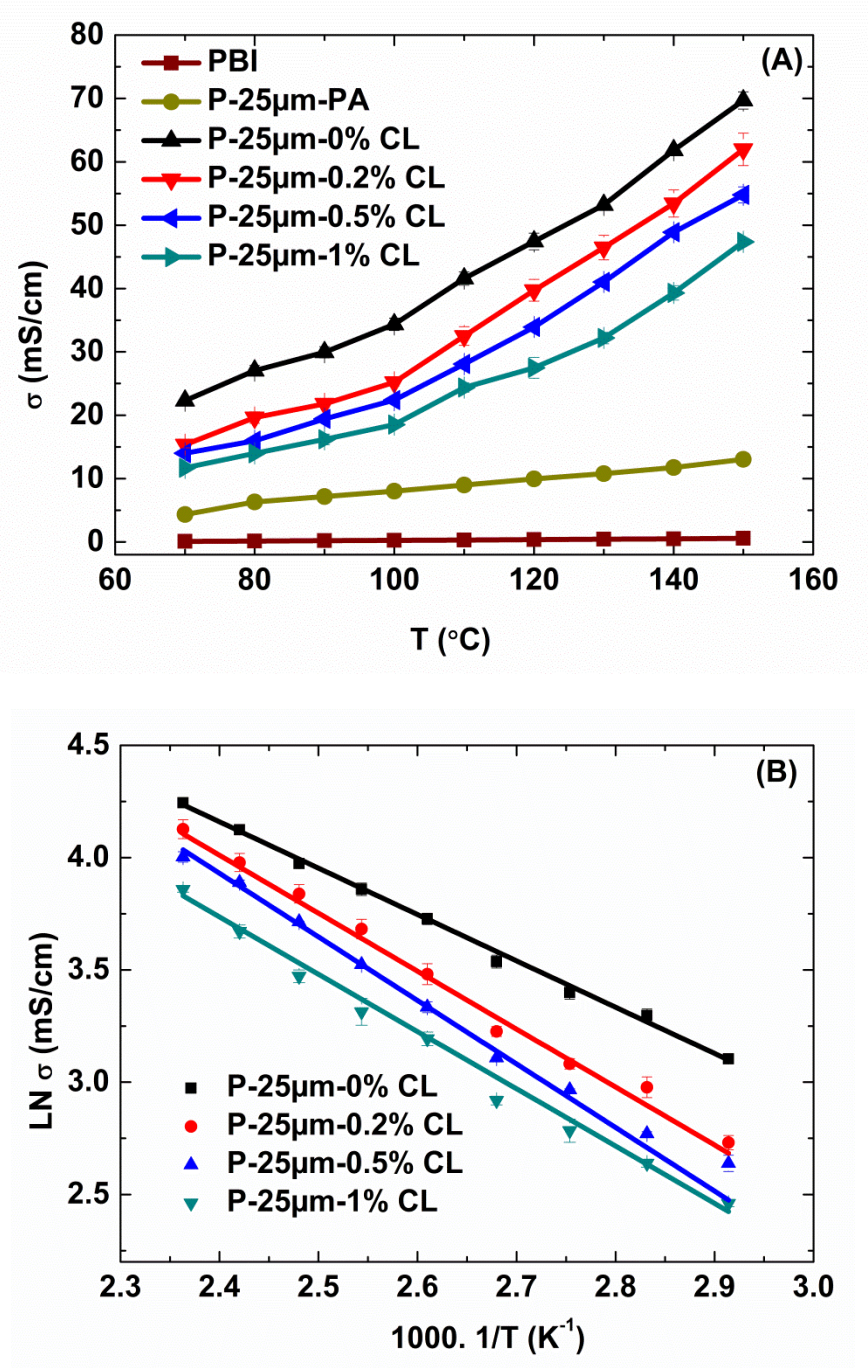

Figure 7. Conductivity measurements for PIL-HPBI membranes as a function of CL content (HPBI-PA and pure PBI are included for the comparison): A) conduction characteristics; B) Arrhenius type plot.

A preliminary assessment on endurance was performed by keeping the PIL-HPBI membranes at 150°C for up to 50 hours (see Figure S6 of the supporting information). In general, all the composite membranes showed performance decay with time on stream; however the effect was more pronounced over non cross-linked samples. The maximum decline in conductivity, ~10.5%, was registered for P-25µm-0%CL; whereas, for P-25µm-1%CL the decrease was only 3.4%. Similar tendency was observed at 200°C, i.e. 4.1% decay for P-25µm-1%CL. The authors hypothesized that such conductivity decrease is related to the rearrangement of the pure PIL skin layer provoked at higher temperatures. Nevertheless, the PIL-HPBI membrane surface revealed unaffected after the durability tests as no cracks or defects were detected visually (see Figure S7 of the supporting information).

3.4.2 Influence of skin layer thickness

For a better insight on the proton transport controlling step through PIL immobilized on asymmetric HPBI microsieves, the proton conductivities of PIL-HPBI obtained from P-15µm microsieves, with 11 µm of skin layer, were also evaluated (see Figure 8). As evidenced, proton conductivity increases with temperature and is also higher for membranes prepared without any CL. The same trend was observed for the thicker P-25 µm derived membranes.

As shown in Figure 8.A, for the conductivity values of PIL-HPBI membranes, for a given CL content, decrease when the skin layer thickness increases. At 150 °C, the proton conductivity of the P-15µm-0%CL membrane (73.5 $mS \cdot cm^{-1}$) is about 4 $mS \cdot cm^{-1}$ higher the value measured for the P-25µm-0%CL membranes with 21 µm thick skin layer. These experimental results could be correlated to the PIL content in the electrolyte membranes: 67.4% for P-15µm-0%CL vs. 63.3% P-25µm-0%CL.

However, it is well known that the overall performance of composite electrolytes is strongly affected not only by the content but also by the distribution of the proton conducting phase

within the membrane. Thus, for a better understanding, the activation energy for proton transport was also evaluated (see Figure 8.B and Table S1 of the supporting information). Whatever the skin layer thickness of the HPBI microsieve support, the obtained Ea values are rather similar. In the case of P-15µm based membranes, the Ea values are 16.8 and 20.6 kJ/mol for P-15µm-0%CL and P-15µm-1%CL respectively; thus rather similar to those measured for P-25µm derived membranes (17.1 kJ/mol for P-25µm-0%CL and 21.8 kJ/mol for P-25µm-1%CL).

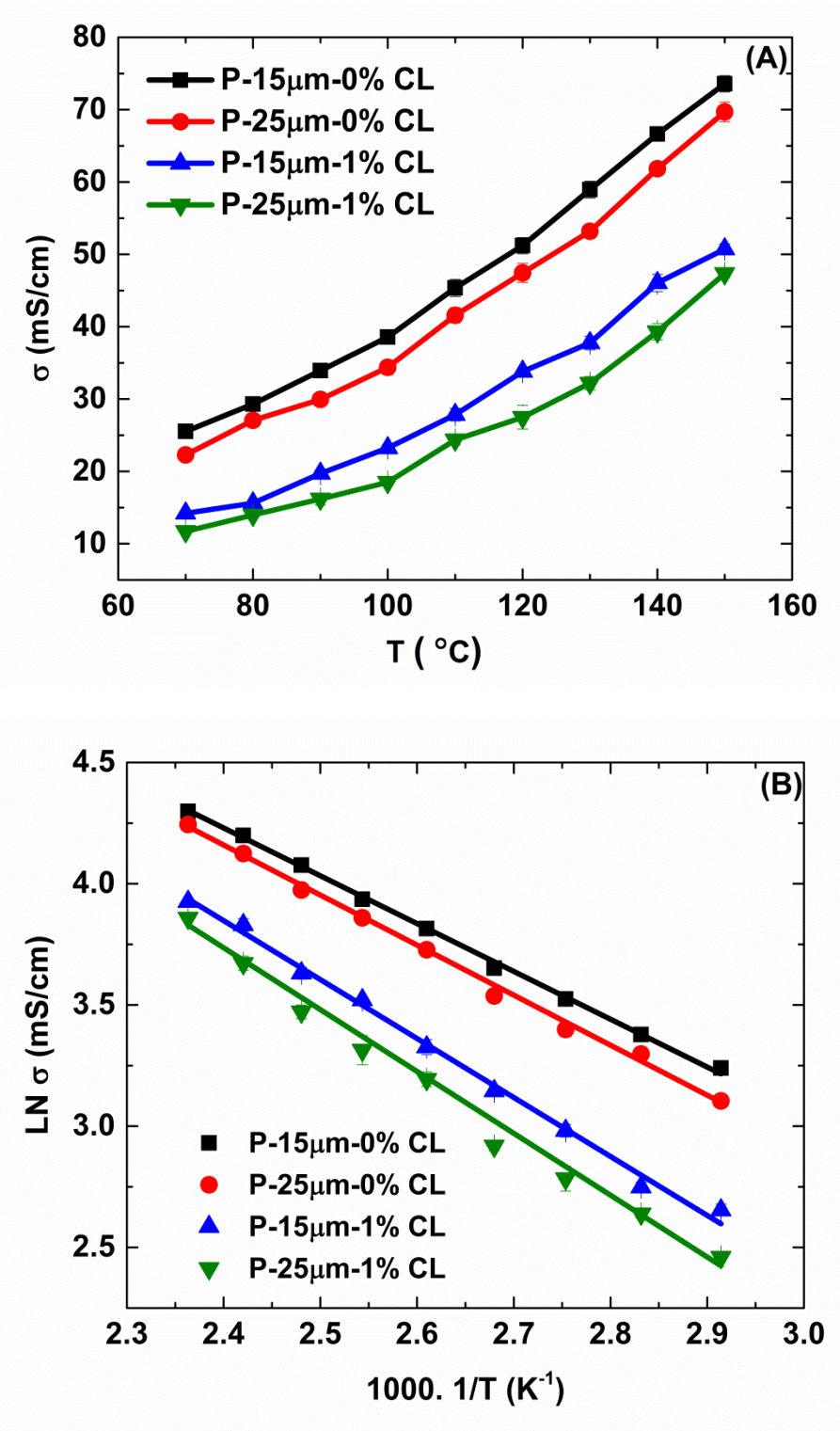

Figure 8. Effect of skin layer thickness on the proton conduction performance of PIL-HPBI membranes with 0% and 1% CL content: A) conductivity values; B) Arrhenius type plot.

Based on the above Ea analysis and considering the membrane asymmetry (see Figure 2 and Figure 3), the hypothesis that the transport of protons through the skin layer is the controlling

step seems plausible. This assumption is also supported by the identical intrinsic porosity of all the HPBI microsieves listed in Table 2 (see SEM cross-section views in Figures 3.D and 3.E). Thus, the PEM membranes prepared from P-25µm microsieves, with 21 µm thick skin layer, lead to slightly lower conductivity values at the expense of improved mechanical properties. According to the above results, the optimal PIL-HPBI formulation as trade-off between proton transport and mechanical resistance corresponds to P-25µm−1%CL.

3.5 Effect of the membrane architecture: comparison with randomly and straight porous PBI supports

Different approaches have been attempted by our group [7, 40] to fabricate PIL-based electrolyte membranes under anhydrous conditions and without any mineral acids while maintaining the mechanical resistance. Our rationale is mainly focused on the selection of the PBI container with adequate pore architecture to improve both the proton transport and the dimensional stability at elevated temperatures.

In this work, the influence of PBI architecture on proton conductivity has been comprehensively examined for the poly[1-(3H-imidazolium)ethylene]bis(trifluoromethanesulfonyl)imide based electrolytes with 1% CL content. The Nyquist plots of all the samples exhibited a compressed arc in the high-frequency region and an inclined straight line indicating that an ion diffusion process at the electrode−electrolyte interface plays an important role (see Figure S8 of the supporting information).

The conduction properties as a function of temperature in the range 70-200 °C, are shown in Figure 9.A for three different PBI supports under anhydrous conditions. These supports are the followings: the herein fully studied hierarchical P-25µm microsieve (HPBI), a dense PBI microsieve [40] (SPBI) having straight pores connecting both sides (17 µm in diameter, 24 µm

thick and 36% porosity), and a randomly porous PBI support (RPBI) having pores in the sub-micrometric range (120 µm thick and 68% in porosity). The derived electrolyte membranes are denoted as PIL-HPBI-1%CL, PIL-SPBI-1%CL and PIL-RPBI-1%CL respectively**.**

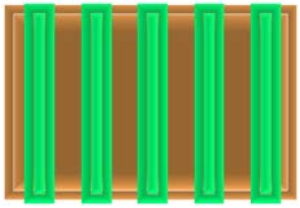

PIL-SPBI

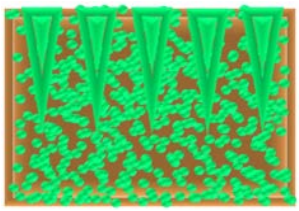

PIL-HPBI

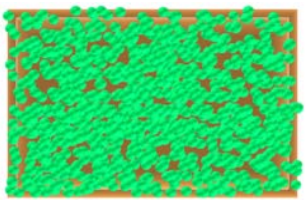

PIL-RPBI

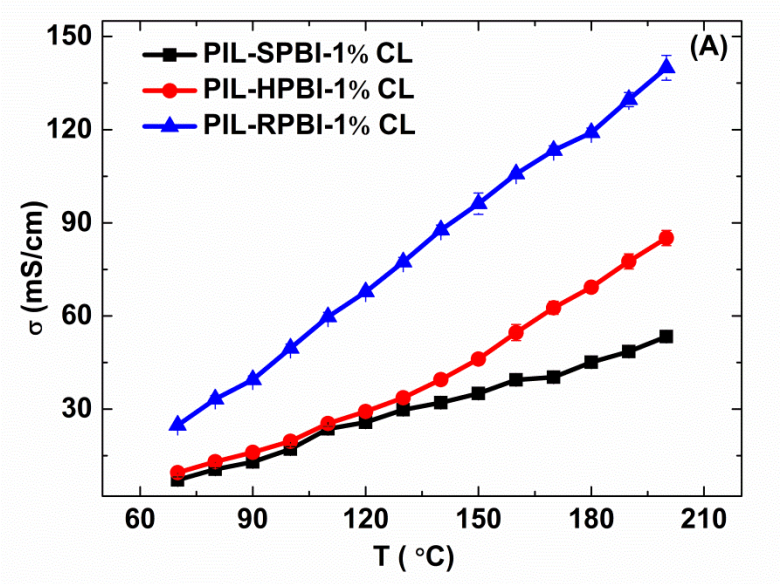

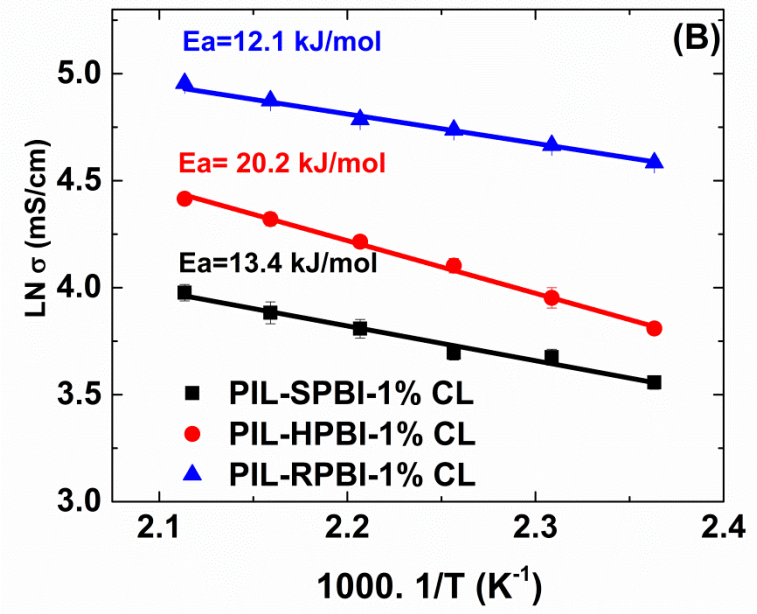

Figure 9. Influence of the PBI support architecture on the conduction performance of PIL-PBI based membranes prepared with 1% cross-linker:A) conductivity values; B) Arrhenius type plot.

Among the tested samples, PIL-RPBI-1%CL electrolyte membrane is most attractive with conductivity as high as 140 $mS \cdot cm^{-1}$. This outperforming behaviour is not only attributed to the high pore volume of the support, providing PIL uptake values up to 86.5 wt % but also to the relevant connectivity of its channels formed during the phase inversion process. Unfortunately this architecture does not provide enough mechanical strength as required for practical operation.

On the other hand, the conductivity values for PIL-HPBI-1%CL (previously referred as P-25µm-1%CL) increased from 47 to 85 $mS \cdot cm^{-1}$ as the temperature increased from 150 to 200 °C. Compared to perforated dense microsieves, i.e. PIL-SPBI-1%CL with 53 $mS \cdot cm^{-1}$ at 200 °C, the proton transport is faster for hierarchical microsieves in spite of lower PIL amount. This result is attributed both to the higher surface area provided by hierarchical microsieves and the porous network connectivity at the straight/intrinsic bulk porosity interface (see graphical abstract).

Thus, the HPBI- architecture leads to an intermediate behaviour in terms of conduction performance; but it is greatly superior in terms of mechanical properties. Overall, such PIL-HPBI electrolyte membranes retain the advantageous features of both as higher and well-connected PIL loadings are achievable without sacrificing the mechanical strength.

The detailed analysis of the apparent Arrhenius-type activation energies for the three different PBI supports is presented in Figure 9.B. The Ea for proton transport via PIL moieties embedded in HPBI support is the highest 20.2 kJ/mol, followed by SPBI and RPBI matrix with 13.4 kJ/mol and 12.1 kJ/mol respectively. This finding corroborates our hypothesis suggesting that proton transport through the intrinsic porosity of the skin layer as controlling step for conduction (see section 3.4.2).

In order to get a further insight on pore morphology, the surface topology of HPBI supports was examined. AFM 3D topography of both HPBI and RPBI supports (used as reference) are compared in Figure 10 (see also Figure S9 of the supporting information). The evaluated roughness values, in the range of a few tens of nanometers, are summarized in Table 5. From these results, it can be concluded that HPBI and RPBI supports exhibit similar surface topology on their both sides.

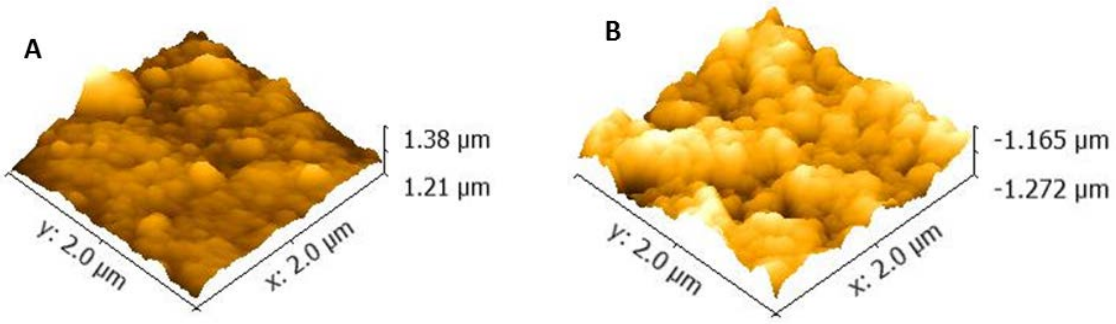

Figure 10. 3D AFM surface images of HPBI-air side (A) and RPBI air side (B).

The microstructure of HPBI and RPBI supports were also analysed by TEM for a proper assessment on their pore connectivity. Images of the cross-section structures are shown in Figure 11 and Figure 12 respectively. As observed, liquid induced phase separation created small pores both at the air side and mold side surfaces; the sizes of these pores are within the roughness values estimated by AFM, i.e. below 50 nm.

Table 5. Surface topology of HPBI and RPBI supports, measured by AFM.

Sample	Average roughness (Ra) (nm)	Square mean roughness (RMS) (nm)
HPBI-Top (Air side)	20.3	25.7
HPBI-Bottom (Mold side)	50.5	67.4
RPBI-Top (Air side)	45.3	55.6
RPBI-Bottom (Glass side)	45.8	56.5

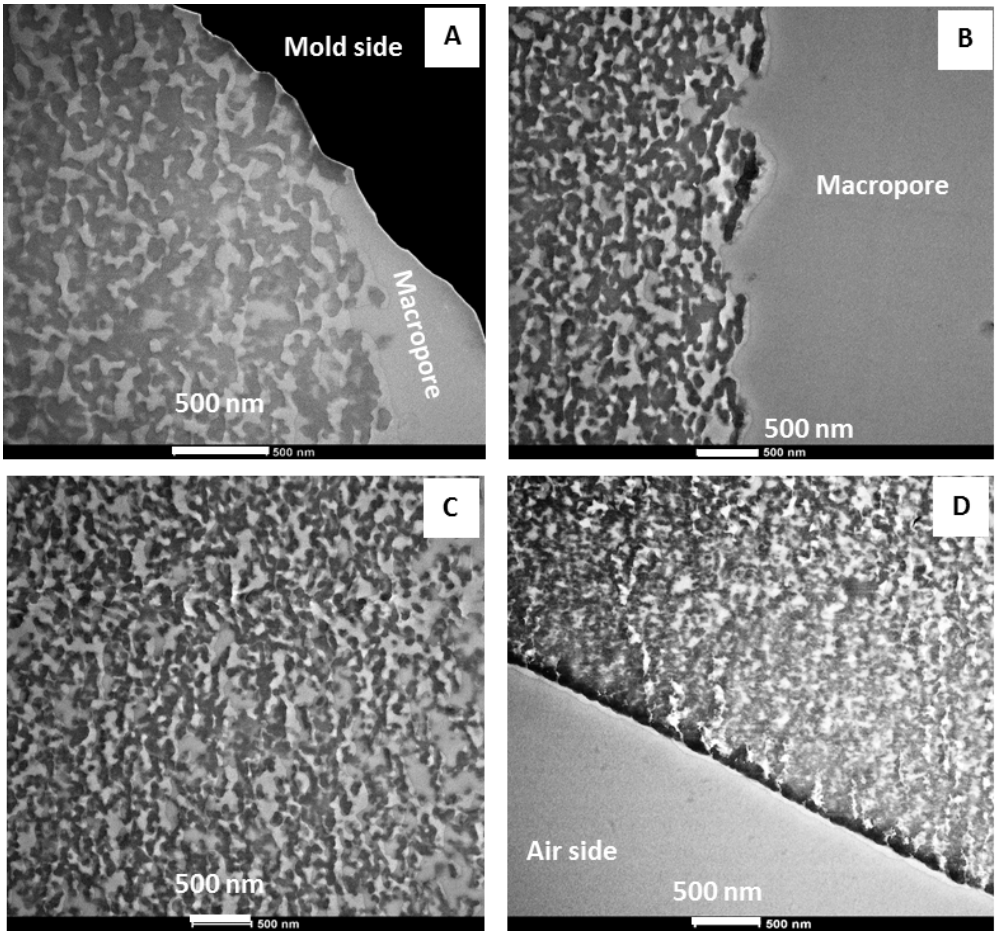

Figure 11. TEM images of the cross-section of HPBI support: (A) mold-side (bottom), (B) straight-intrinsic porosity interface, (C) Intrinsic porosity of the skin layer, (D) air side (top).

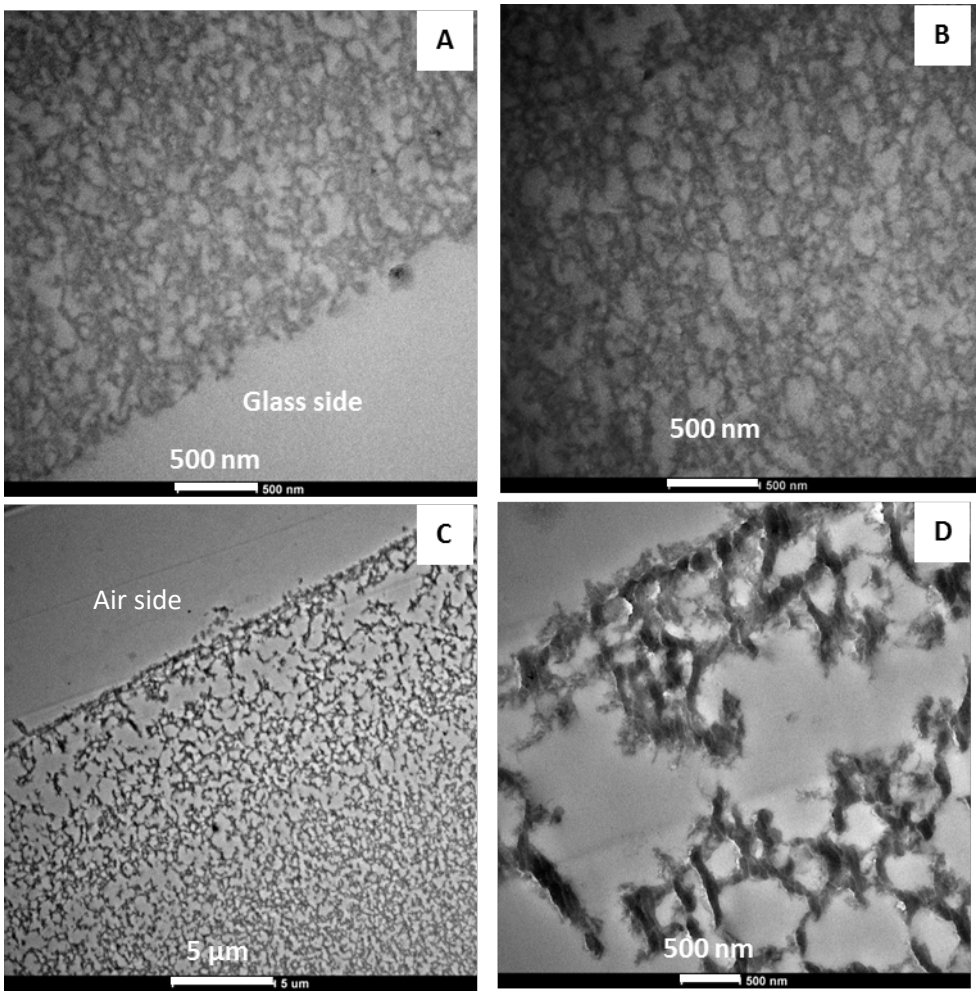

Figure 12. TEM images of the cross-section of RPBI support: (A) glass side (bottom), (B) Middle part, (C) air side (top), (D) air side at higher magnification.

TEM observations reveal that the intrinsic pores of both HPBI and RPBI polymeric matrix are completely different in size and morphology, supporting the measured Ea values previously discussed (see Figure 9.B). A highly porous structure with closed-cell intrinsic pores with sizes between 0.2 µm and 2.0 µm (preferentially located near the air side, see Figure 12 C-D) is formed during phase inversion of RPBI [7]. The conduction pattern on PIL channels for RPBI/PIL-1%CL is almost unaffected by the substrate wall−PIL interactions. In

fact, the registered Ea values resembles those previously reported for unsupported PIL-1%CL, i.e. 12.3 kJ/mol [40].

Particularly remarkable is the porous structure of the straight macropore wall surface in the HPBI support (see Figure 11. A-B). Over this area, well-connected pores at the straight macropore/intrinsic porosity interface are clearly distinguished. In addition, worm-shape pores below 0.2 µm in size are predominant along the whole thickness (see Figure 11. A-D). Unlike previously, the interactions of PIL molecules with the walls of the confining intrinsic PBI pores are not negligible. These pore-wall-fluid interactions anticipated by FTIR analyses (see section 3.2) slow down the proton transport dynamics and subsequently provokes an increase of Ea.

4. CONCLUSIONS

This work presents a feasible strategy to construct hierarchical PIL channels into a PBI matrix. Low- cost outperforming PEMs for prolonged operation at temperatures up to 200 °C under anhydrous conditions and in absence of mineral acids have been successfully developed. These results pave the way for the future development of high temperature flexible electrolytes for electrochemical devices.

ASSOCIATED CONTENT

Supporting Information

Casting device and procedure for MIL infiltration on HPBI microsieves. Proton Conductivity Determination from the Nyquist plots: P-25µm-0%CL analyses and comparison of electrolyte resistance vs. polarization resistance. Stress–strain curves of PIL-HPBI membranes. Replica conductivity measurements. Analysis of Activation Energy for proton transport as a function

of CL content and skin layer thickness. Conduction performance as a function of time on stream at 150°C and 200°C. Physical Appearance of PIL-HPBI electrolye membranes before and after testing. Nyquist plots for PIL supported on different PBI containers. Analysis of the surface topology by AFM of HPBI microsieve and randomly porous PBI support.

This information is available free of charge via the Internet at http://pubs.acs.org.

AUTHOR INFORMATION

Corresponding Author

*E-mail: mapina@unizar.es; Tel: +34 976 761155

ACKNOWLEDGMENTS

The authors would like to acknowledge the financial support from the Government of Aragon and the Education, Audiovisual and Culture Executive Agency (EU-EACEA) within the EUDIME – “Erasmus Mundus Doctorate in Membrane Engineering” program (FPA 2011-0014, SGA 2012-1719, http://eudime.unical.it). CIBER-BBN is an initiative funded by the VI National R&D&i Plan 2008−2011 financed by the Instituto de Salud Carlos III with the assistance of the European Regional Development Fund. Authors acknowledge the LMA-INA for offering access to their instruments and expertise. The authors would like to thankDr. Celine Pochat-Bohatier and Sakthivel Nagarajan (IEM, Montpellier) for their help in the mechanical characterization.

REFERENCES

1. Debe, M. K. Electrocatalyst Approaches and Challenges for Automotive Fuel cells. *Nature* **2012,** *486*, 43-51.

2. Liu, S.; Zhou, L.; Wang, P.; Zhang, F.; Yu, S.; Shao, Z.; Yi, B. Ionic-Liquid-based Proton Conducting Membranes for Anhydrous H2/Cl2 Fuel-cell applications. *ACS Appl.Mater. Interfaces* **2014,** *6*, 3195-3200.
3. Peighambardoust, S. J.; Rowshanzamir, S.; Amjadi, M. Review of the Proton Exchange Membranes for Fuel cell Applications. *Int. J. Hydrogen Energy* **2010,** *35*, 9349-9384.
4. Wainright, J. S.; Wang, J. T.; Weng, D.; Savinell, R. F.; Litt, M. Acid-Doped Polybenzimidazoles: A New Polymer Electrolyte. *J. Electrochem.Soc.* **1995,** *142*, L121-L123.
5. Li, Q.; Jensen, J. O.; Savinell, R. F.; Bjerrum, N. J. High Temperature Proton Exchange Membranes based on Polybenzimidazoles for Fuel cells. *Prog. Polym.Sci.* **2009,** *34*, 449-477.
6. Li, Q.; He, R.; Jensen, J. O.; Bjerrum, N. J. Approaches and Recent Development of Polymer Electrolyte Membranes for Fuel Cells Operating above 100 °C. *Chem. Mater.* **2003,** *15*, 4896-4915.
7. Lemus, J.; Eguizábal, A.; Pina, M. P. Endurance Strategies for the Preparation of High Temperature Polymer Electrolyte Membranes by UV polymerization of 1-H-3-vinylimidazolium bis(trifluoromethanesulfonyl)imide for Fuel cell Applications. *Int. J. Hydrogen Energy* **2016,** *41*, 3981-3993.
8. Jheng, L.-C.; Hsu, S. L.-C.; Tsai, T.-Y.; Chang, W. J.-Y. A Novel Asymmetric Polybenzimidazole Membrane for High Temperature Proton Exchange Membrane Fuel cells. *J. Mater. Chem. A* **2014,** *2*, 4225-4233.
9. Wang, J. T.-W.; Hsu, S. L.-C. Enhanced High-Temperature Polymer Electrolyte Membrane for Fuel cells based on Polybenzimidazole and Ionic Liquids. *Electrochim. Acta* **2011,** *56*, 2842-2846.
10. Van de Ven, E.; Chairuna, A.; Merle, G.; Benito, S. P.; Borneman, Z.; Nijmeijer, K. Ionic Liquid Doped Polybenzimidazole Membranes for High Temperature Proton Exchange Membrane fuel cell Applications. *J. Power Sources* **2013,** *222*, 202-209.
11. Hazarika, M.; Jana, T. Proton Exchange Membrane Developed from Novel Blends of Polybenzimidazole and Poly(vinyl-1,2,4-triazole). *ACS Appl.Mater. Interfaces* **2012,** *4*, 5256-5265.
12. Dahi, A.; Fatyeyeva, K.; Langevin, D.; Chappey, C.; Rogalsky, S. P.; Tarasyuk, O. P.; Marais, S. Polyimide/ionic liquid Composite Membranes for Fuel cells Operating at High Temperatures. *Electrochim. Acta* **2014,** *130*, 830-840.
13. Lalia, B. S.; Sekhon, S. S. Polymer Electrolytes containing Ionic Liquids with Acidic Counteranion (DMRImH2PO4, R = ethyl, butyl and octyl). *Chem. Phys. Lett.* **2006,** *425*, 294-300.
14. Tiyapiboonchaiya, C.; Pringle, J. M.; Sun, J.; Byrne, N.; Howlett, P. C.; MacFarlane, D. R.; Forsyth, M. The Zwitterion Effect in High-Conductivity Polyelectrolyte Materials. *Nat. Mater.* **2004,** *3*, 29-32.
15. Ye, H.; Huang, J.; Xu, J. J.; Kodiweera, N. K. A. C.; Jayakody, J. R. P.; Greenbaum, S. G. New Membranes based on Ionic Liquids for PEM Fuel cells at Elevated Temperatures. *J. Power Sources* **2008,** *178*, 651-660.
16. Lin, B.; Cheng, S.; Qiu, L.; Yan, F.; Shang, S.; Lu, J. Protic Ionic Liquid-Based Hybrid Proton-Conducting Membranes for Anhydrous Proton Exchange Membrane Application. *Chem. Mater.* **2010,** *22*, 1807-1813.
17. Lemus, J.; Eguizábal, A.; Pina, M. P. UV Polymerization of Room Temperature Ionic Liquids for High Temperature PEMs: Study of Ionic Moieties and Crosslinking Effects. *Int. J. Hydrogen Energy* **2015,** *40*, 5416-5424.

18. Eguizábal, A.; Lemus, J.; Pina, M. P. On the Incorporation of Protic Ionic Liquids Imbibed in Large Pore Zeolites to Polybenzimidazole Membranes for High Temperature Proton Exchange Membrane Fuel cells. *J. Power Sources* **2013,** *222*, 483-492.
19. Hopkinson, D.; Zeh, M.; Luebke, D. The bubble point of Supported Ionic liquid Membranes using Flat sheet Supports. *J. Membr. Sci.* **2014,** *468*, 155-162.
20. Li, M.; Yang, L.; Fang, S.; Dong, S. Novel Polymeric Ionic Liquid Membranes as Solid Polymer Electrolytes with High Ionic Conductivity at Moderate Temperature. *J. Membr. Sci.* **2011,** *366*, 245-250.
21. Mecerreyes, D. Polymeric Ionic Liquids: Broadening the Properties and Applications of Polyelectrolytes. *Prog. Polym.Sci.* **2011,** *36*, 1629-1648.
22. Díaz, M.; Ortiz, A.; Vilas, M.; Tojo, E.; Ortiz, I. Performance of PEMFC with New Polyvinyl-ionic Liquids based Membranes as Electrolytes. *Int. J. Hydrogen Energy* **2014,** *39*, 3970-3977.
23. Iojoiu, C.; Martinez, M.; Hanna, M.; Molmeret, Y.; Cointeaux, L.; Leprêtre, J.-C.; Kissi, N. E.; Guindet, J.; Judeinstein, P.; Sanchez, J.-Y. PILs-based Nafion Membranes: a route to High-Temperature PEFMCs dedicated to Electric and Hybrid Vehicles. *Polym. Adv. Technol.* **2008,** *19*, 1406-1414.
24. Pont, A.-L.; Marcilla, R.; De Meatza, I.; Grande, H.; Mecerreyes, D. Pyrrolidinium-based Polymeric Ionic Liquids as Mechanically and Electrochemically Stable Polymer Electrolytes. *J. Power Sources* **2009,** *188*, 558-563.
25. Liang, B.; Jiang, Q.; Tang, S.; Li, S.; Chen, X. Porous Polymer Electrolytes with High Ionic Conductivity and Good Mechanical Property for Rechargeable Batteries. *J. Power Sources* **2016,** *307*, 320-328.
26. Eguizábal, A.; Lemus, J.; Urbiztondo, M.; Garrido, O.; Soler, J.; Blazquez, J. A.; Pina, M. P. Novel Hybrid Membranes based on Polybenzimidazole and ETS-10 titanosilicate type Material for High Temperature Proton Exchange Membrane Fuel cells: A Comprehensive Study on Dense and Porous Systems. *J. Power Sources* **2011,** *196*, 8994-9007.
27. Kuiper, S.; van Rijn, C. J. M.; Nijdam, W.; Elwenspoek, M. C. Development and Applications of Very High Flux Microfiltration Membranes. *J. Membr. Sci.* **1998,** *150*, 1-8.
28. Gielens, F. C.; Tong, H. D.; van Rijn, C. J. M.; Vorstman, M. A. G.; Keurentjes, J. T. F. Microsystem Technology for High-flux Hydrogen Separation Membranes. *J. Membr. Sci.* **2004,** *243*, 203-213.
29. H. D. Tong, F. C. G., J. G. E. Gardeniers, H. V. Jansen, C. J. M. van Rijn,; M. C. Elwenspoek, a. W. N. Microfabricated Palladium-Silver Alloy Membranes and Their Applications in Hydrogen Separation. *Ind. Eng. Chem. Res.* **2004,** *43*, 4182-4187.
30. Kniazeva, T.; Hsiao, J. C.; Charest, J. L.; Borenstein, J. T. A Microfluidic Respiratory assist Device with High Gas permeance for Artificial Lung Applications. *Biomed. Microdevices* **2011,** *13*, 315-323.
31. Bikel, M.; Çulfaz, P. Z.; Bolhuis-Versteeg, L. A. M.; Pérez, J. G.; Lammertink, R. G. H.; Wessling, M. Polymeric Microsieves via Phase Separation Microfabrication: Process and Design Optimization. *J. Membr. Sci.* **2010,** *347*, 93-100.
32. Carstensen, F.; Kasperidus, T.; Wessling, M. Overcoming the Drawbacks of Microsieves with Micromeshes for In situ product recovery. *J. Membr. Sci.* **2013,** *436*, 16-27.
33. Vogelaar, L.; Lammertink, R. G.; Barsema, J. N.; Nijdam, W.; Bolhuis-Versteeg, L. A.; van Rijn, C. J.; Wessling, M. Phase Separation Micromolding: A new Generic Approach for Microstructuring Various Materials. *Small* **2005,** *1*, 645-655.
34. Yan, F.; Ding, A.; Girones, M.; Lammertink, R. G.; Wessling, M.; Borger, L.; Vilsmeier, K.; Goedel, W. A. Hierarchically Structured Assembly of Polymer Microsieves, made by a Combination of Phase Separation Micromolding and Float-casting. *Adv. Mater.* **2012,** *24*, 1551-1557.

35. Gironès, M.; Akbarsyah, I. J.; Nijdam, W.; van Rijn, C. J. M.; Jansen, H. V.; Lammertink, R. G. H.; Wessling, M. Polymeric Microsieves Produced by Phase Separation Micromolding. *J. Membr. Sci.* **2006,** *283*, 411-424.
36. Vogelaar, L.; Barsema, J. N.; van Rijn, C. J. M.; Nijdam, W.; Wessling, M. Phase Separation Micromolding—PSμM. *Adv. Mater.* **2003,** *15*, 1385-1389.
37. Vriezekolk, E. J.; Kemperman, A. J. B.; Gironès, M.; de Vos, W. M.; Nijmeijer, K. A Solvent-Shrinkage Method for Producing Polymeric Microsieves with Sub-micron size Pores. *J. Membr. Sci.* **2013,** *446*, 10-18.
38. Wu, C.-G.; Lu, M.-I.; Chuang, H.-J. PVdF-HFP/P123 Hybrid with Mesopores: A New Matrix for High-Conducting, Low-leakage Porous Polymer Electrolyte. *Polymer* **2005,** *46*, 5929-5938.
39. Eguizábal, A.; J.Lemus; Roda, V.; Urbiztondo, M.; Barreras, F.; Pina, M. P. Nanostructured Electrolyte Membranes based on Zeotypes, Protic Ionic Liquids and Porous PBI membranes: Preparation, Characterization and MEA testing. *Int. J. Hydrogen Energy* **2012,** *37*, 7221-7234.
40. Kallem, P.; Eguizábal, A.; Mallada, R.; and Pina, M. P., Constructing Straight Poly-Ionic liquid Microchannels for Fast Anhydrous Proton transport. *ACS Appl. Mater. Interfaces* **2016,** *8*, 35377-35389.
41. Howlett, P. C.; Brack, N.; Hollenkamp, A. F.; Forsyth, M.; MacFarlane, D. R. Characterization of the Lithium Surface in N-Methyl-N-alkylpyrrolidinium Bis(trifluoromethanesulfonyl)amide Room-Temperature Ionic Liquid Electrolytes. *J. Electrochem. Soc.* **2006,** *153*, A595.
42. Rewar, A. S.; Chaudhari, H. D.; Illathvalappil, R.; Sreekumar, K.; Kharul, U. K. New Approach of Blending Polymeric Ionic Liquid with Polybenzimidazole (PBI) for Enhancing Physical and Electrochemical Properties. *J. Mater. Chem. A* **2014,** *2*, 14449-14458.
43. Bauer, F.; Denneler, S.; Willert-Porada, M. Influence of Temperature and Humidity on the Mechanical Properties of Nafion® 117 Polymer Electrolyte Membrane. *J. Polym. Sci., Part B: Polym. Phys.* **2005,** *43*, 786-795.
44. Rodgers, M. P.; Berring, J.; Holdcroft, S.; Shi, Z. The Effect of Spatial Confinement of Nafion® in Porous Membranes on Macroscopic Properties of the Membrane. *J. Memb. Sci.* **2008,** *321*, 100-113.
45. Fang, J.; Lyu, M.; Wang, X.; Wu, Y.; Zhao, J. Synthesis and Performance of Novel Anion Exchange Membranes based on Imidazolium Ionic Liquids for Alkaline Fuel cell Applications. *J. Power Sources* **2015,** *284*, 517-523.
46. Li, Q.; He, R.; Jensen, J. O.; Bjerrum, N. J. PBI-based Polymer Membranes for High Temperature Fuel Cells – Preparation, Characterization and Fuel Cell Demonstration. *Fuel Cells* **2004,** *4*, 147-159.
47. Li, Q.; He, R.; Berg, R. W.; Hjuler, H. A.; Bjerrum, N. J. Water uptake and Acid Doping of Polybenzimidazoles as Electrolyte Membranes for Fuel cells. *Solid State Ionics* **2004,** *168*, 177-185.
48. Ma, Y. L.; Wainright, J. S.; Litt, M. H.; Savinell, R. F. Conductivity of PBI Membranes for High-Temperature Polymer Electrolyte Fuel Cells. *J. Electrochem. Soc.* **2004,** *151*, A8-A16.
49. Lobato, J.; Cañizares, P.; Rodrigo, M. A.; Linares, J. J.; Aguilar, J. A. Improved Polybenzimidazole Films for H3PO4-doped PBI-based High Temperature PEMFC. *J. Membr. Sci.* **2007,** *306*, 47-55.
50. Vengatesan, S.; Santhi, S.; Sozhan, G.; Ravichandran, S.; Davidson, D. J.; Vasudevan, S. Novel Cross-linked Anion Exchange Membrane based on Hexaminium Functionalized Poly(vinylbenzyl chloride). *RSC Adv.* **2015,** *5*, 27365-27371.

51. Li, H.-Y.; Liu, Y.-L. Polyelectrolyte Composite Membranes of Polybenzimidazole and Crosslinked Polybenzimidazole-polybenzoxazine Electrospun Nanofibers for Proton Exchange Membrane Fuel Cells. *J. Mater. Chem. A* **2013,** *1*, 1171-1178.
52. Mamlouk, M.; Ocon, P.; Scott, K. Preparation and Characterization of Polybenzimidzaole/diethylamine Hydrogen Sulphate for Medium Temperature Proton Exchange Membrane Fuel cells. *J. Power Sources* **2014,** *245*, 915-926.
53. Chopade, S. A.; So, S.; Hillmyer, M. A.; Lodge, T. P. Anhydrous Proton Conducting Polymer Electrolyte Membranes via Polymerization-Induced Microphase Separation. *ACS Appl. Mater. Interfaces* **2016,** *8*, 6200-6210.

Graphic for manuscript